scientific reports

Check for updates

OPEN

Abiotic and biotic factors controlling the dynamics of soil respiration in a coastal dune ecosystem in western Japan

Munemasa Teramoto[1]✉, Toru Hamamoto[1,2], Naishen Liang[3], Takeshi Taniguchi[1], Takehiko Y. Ito[4], Richa Hu[5] & Norikazu Yamanaka[1]

In this study, we examined the abiotic and biotic factors controlling the dynamics of soil respiration (R_s) while considering the zonal distribution of plant species in a coastal dune ecosystem in western Japan, based on periodic R_s data and continuous environmental data. We set four measurement plots with different vegetation compositions: plot 1 on bare sand; plot 2 on a cluster of young *Vitex rotundifolia* seedlings; plot 3 on a mixture of *Artemisia capillaris* and *V. rotundifolia*; and plot 4 on the inland boundary between the coastal vegetation zone and a *Pinus thunbergii* forest. R_s increased exponentially along with the seasonal rise in soil temperature, but summer drought stress markedly decreased R_s in plots 3 and 4. There was a significant positive correlation between the natural logarithm of belowground plant biomass and R_s in autumn. Our findings indicate that the seasonal dynamics of R_s in this coastal dune ecosystem are controlled by abiotic factors (soil temperature and soil moisture), but the response of R_s to drought stress in summer varied among plots that differed in dominant vegetation species. Our findings also indicated that the spatial dynamics of R_s are mainly controlled by the distribution of belowground plant biomass and autotrophic respiration.

Coastal dunes are important ecosystems that are inhabited by unique vegetation communities, but they are being threatened by the recent climate change and developmental pressures[1]. On the other hand, coastal dune ecosystems are gaining attention as green infrastructure that can provide many kinds of ecosystem services[2], including carbon sequestration and storage[3]. A soil carbon analysis by Drius et al.[4] suggested that Italian coastal dunes in the Natura 2000 network are carbon sinks. We have limited information, however, on the carbon cycle in coastal dune ecosystems based on CO_2 flux observation data. Therefore, more CO_2 flux research in coastal dunes is needed to clarify the value of coastal dune ecosystems from the viewpoint of climate change mitigation. This new information may also contribute to protecting dune ecosystems and establishing sustainable management strategies for these vulnerable ecosystems.

Soil respiration (R_s) is the second-largest carbon flux in terrestrial ecosystems and a major component of the global carbon cycle[5]. R_s consists of heterotrophic respiration (R_h, decomposition of plant litter and soil organic carbon (SOC) by microbiota) and autotrophic respiration (R_a) that comes from plant roots, mycorrhiza, and other rhizosphere microorganisms[6]. Although several studies have estimated global R_s[5,7], large uncertainty in the estimation still remains[8] and may be partly explained by spatial bias for R_s[9]. Not only spatial bias but also bias associated with ecosystem types might contribute to the uncertainty. For example, according to the recent database of R_s by Jian et al.[10], R_s data in forest ecosystems (especially in temperate regions) is the most frequently recorded category from the viewpoint of the number of data in the database. More research in a wider array of ecosystems, however, would help improve R_s estimation as well as our understanding of the mechanism underlying the R_s response to environmental factors.

In most ecosystems, abiotic factors such as soil temperature and soil moisture are the major environmental factors controlling the dynamics of R_s, but the magnitude and the direction (increase or decrease) of the R_s response to those factors vary among ecosystems. Generally, R_s increases exponentially along with a rise in soil

[1]Arid Land Research Center, Tottori University, Hamasaka, Tottori 680-0001, Japan. [2]Graduate School of Agricultural Science, Tohoku University, Sendai, Miyagi 980-8572, Japan. [3]Earth System Division, National Institute for Environmental Studies, Tsukuba, Ibaraki 305-8506, Japan. [4]International Platform for Dryland Research and Education, Tottori University, Hamasaka, Tottori 680-0001, Japan. [5]The United Graduate School of Agricultural Sciences, Tottori University, Koyama-Minami, Tottori 680-8553, Japan. ✉email: teramoto.m@tottori-u.ac.jp

temperature[11–13], whereas R_s has a "mountain-shaped" relationship with soil moisture, because conditions that are too dry or too wet suppress R_s[14]. Gao et al.[15] observed an exponential relationship between soil temperature and R_s in plantation forests and a secondary forest in coastal dunes, as typically observed in other terrestrial ecosystems; they also reported that soil moisture was positively related to R_s in several stands among the study sites. Their findings suggest that soil temperature and soil moisture also exert strong control over the seasonal dynamics of R_s in coastal dunes.

In addition to abiotic factors, biotic factors are also reported to regulate the dynamics of R_s in coastal dune ecosystems. Previous studies suggested that biotic factors like root biomass and microbial population were also important indicators for the dynamics of R_s in coastal dune ecosystems[15,16], however, it needs more discussion to get a consensus about which biotic factor is the most dominant one. Chapman[17] estimated that 70% of R_s is caused by root respiration, based on surveys in several heathland ecosystems that included dune-heath ecosystems, suggesting a strong influence of vegetation on R_s in those ecosystems. Because coastal dune ecosystems are generally carbon-limited, interactions between vegetation and R_s might be more clearly observed than in other ecosystems.

In coastal dune ecosystems, a zonal distribution (zonation) of coastal plant species with distance from the shoreline is typically observed[18]. As the distance from the shoreline increases, the vegetation gradually changes from herbs to shrubs and tree species[4,19], and the amount of soil organic matter is also positively correlated with the distance[20]. Because plant communities can be a strong driver of R_s[21], the dynamics of R_s and the response to environmental factors may differ between vegetation zones. Thus, for a better understanding of R_s dynamics and the mechanism underlying the R_s response to abiotic and biotic factors in coastal dune ecosystems, it is necessary to account for the zonal distribution of plant communities. No study has yet examined, however, if the R_s dynamics and responses to abiotic and biotic factors differ among plots dominated by different coastal plant species.

In this study, we investigated the dynamics of R_s in a Japanese coastal dune ecosystem focusing on abiotic factors (soil temperature and soil moisture) and biotic factors (belowground plant biomass and microbial abundance), while considering the difference in dominant coastal vegetation. We hypothesized that the relationships between the controlling factors (abiotic and biotic) and R_s vary among plots dominated by different vegetation species. We also aimed to identify the mechanism(s) that caused the difference in the response of R_s using ecological and microbial analysis.

Results

Environmental data. The time series of the soil moisture at a depth of 30 cm and soil temperature at depths of 0–5, 5, 10, 30, and 50 cm are shown in Fig. 1a. The maximum soil temperature from June to December 2020 at 0–5 cm, based on data collected at each measurement point during each R_s measurement, was 65.0 °C measured during the daytime in late August. The maximum soil temperatures based on the average of 30-min continuous measurements at depths of 5, 10, 30, and 50 cm were 49.7, 40.1, 33.2, and 30.4 °C, respectively, in late August. The minimum soil temperature from June to December 2020 at 0–5 cm during R_s measurement was 9.3 °C during the daytime in mid-November. The minimum soil temperature at depths of 5, 10, 30, and 50 cm was 0.6, 0.9, 2.2, and 3.7 °C, respectively, in late December.

The maximum average soil moisture at the depth of 30 cm was 19.0% in the middle of June, the early summer rainy season, and the minimum value was 1.6% in early September (Fig. 1a). The remarkable decrease in soil moisture was due to limited precipitation in August. The monthly precipitation recorded at the meteorological observatory in Tottori (Japan Meteorological Agency) in August was 8.5 mm, the lowest monthly precipitation in August in the last 50 years.

Dynamics of R_s in each plot. R_s values in plots 1–3 peaked at the end of July to early August, whereas R_s in plot 4 peaked in the middle of June (Fig. 1b). The maximum R_s values were 1.82 ± 0.05, 2.95 ± 0.10, 1.63 ± 0.14, and 1.99 ± 0.18 μmol CO_2 m^{-2} s^{-1} in plots 1 to 4, respectively (mean ± SE, $n = 10$). Minimum R_s values in each plot were observed from mid-November to early December and were 0.11 ± 0.004, 0.61 ± 0.08, 0.23 ± 0.05, and 0.58 ± 0.08 μmol CO_2 m^{-2} s^{-1} in plots 1–4, respectively (mean ± SE, $n = 10$). In plots 3 and 4, R_s was also markedly decreased at the end of August. During the measurement period from 15 June to 2 December (13 R_s measurements), the average R_s value in each plot was 1.35 ± 0.53, 2.03 ± 0.67, 1.07 ± 0.50, and 1.27 ± 0.45 μmol CO_2 m^{-2} s^{-1}, respectively (mean ± SD).

Soil temperature and soil moisture response of R_s. R_s increased exponentially along with the seasonal rise in soil temperature, except for late August, and the goodness of fit (R^2) was best at a depth of 50, 50, 10, and 0–5 cm in plots 1–4, respectively (Fig. 2). In this study, we selected the soil temperature at the depth of 30 cm as the standard for analysis of R_s. Significant exponential relationships between 30-cm soil temperature and R_s were observed in plots 1, 2, and 3 when we used all data (Fig. 3, $p < 0.001$ in plots 1 and 2, $p = 0.022$ in plot 3), whereas there was no significant exponential relationship between soil temperature and R_s in plot 4 ($p = 0.344$). However, if we excluded data collected in late August (21 and 28 August), the drought period, a significant exponential relationship was also confirmed in plot 4 (Fig. 3, $p = 0.006$).

Using the soil temperature response curve of R_s for which data in late August (drought period) were excluded, we analyzed the relationships between soil moisture at a depth of 30 cm and temperature-normalized R_s (R_{sN}) in each plot. These relationships were significant in plot 3 ($p = 0.025$) and plot 4 ($p = 0.002$, Fig. 4), but they were not significant in plot 1 ($p = 0.232$) or plot 2 ($p = 0.055$). Ranges of R_{sN} during the drought period from plots 1 to 4 were 0.76–0.83, 0.75–0.82, 0.35–0.45, and 0.33–0.44, respectively (Fig. 4).

Belowground plant biomass. We observed a large variation in the distribution of total belowground plant biomass (BPB) and rooting depth in each plot (Fig. 5). Total BPB to a depth of 220 cm was 483.8, 1604.6,

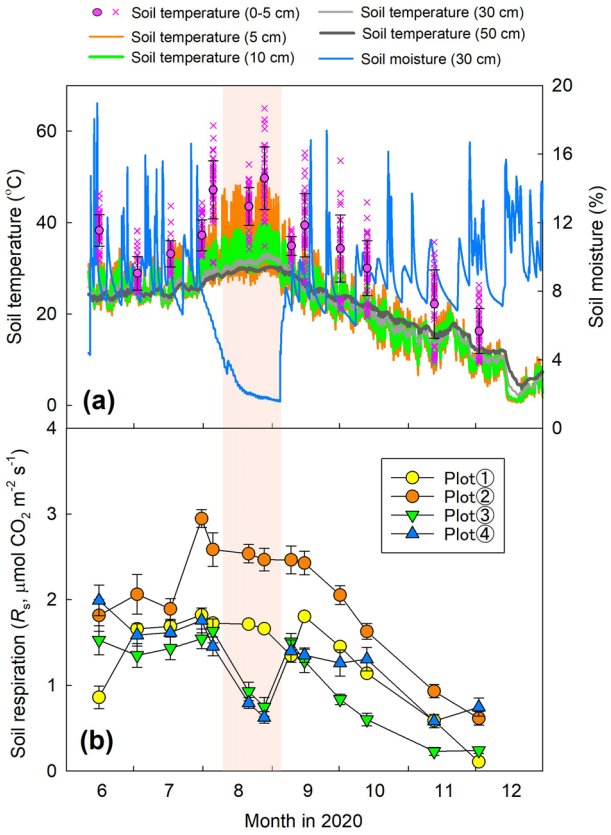

Figure 1. (**a**) Seasonal dynamics of soil moisture at a depth of 30 cm (averaged value of CS616 sensors in plots 1, 3, and 4) and soil temperature at depths of 0–5, 5, 10, 30, and 50 cm; (**b**) seasonal dynamics of R_s in each measurement plot. The soil temperature at the depth of 0–5 cm for all 40 measurement points in plots 1–4 is shown by pink crosses, and the average value (mean ± SD) during the daytime is shown by pink circles. Soil temperature at depths of 5, 10, and 30 cm is the average value of reference soil temperature (thermocouple) at the center of plot 3 and stand-alone soil temperature sensors in plots 1 and 4. Soil temperature at a depth of 50 cm is the reference soil temperature at the center of plot 3. Bars in (**b**) show the standard error of the mean ($n = 10$). The area of light orange represents the drought period (10 August to 4 September) when the daily averaged soil moisture was less than 3.9%, the threshold soil moisture value. This figure was created using Sigmaplot 14.5 software (Systat Software, San Jose, CA, USA, https://systatsoftware.com/sigmaplot/).

751.2, and 552.3 g m^{-2} for plots 1–4, respectively ($n = 1$). The majority of BPB was concentrated in the upper 30 cm in plot 3 (82%) and plot 4 (95%), and the BPB ratios to a depth of 50 cm were 93% (plot 3) and 98% (plot 4), respectively. In contrast, the BPB ratios in the upper 30 cm in plots 1 and 2 were both 14%, and the BPB ratios to a depth of 50 cm were both 26%.

Influence of BPB on R_s. There was no significant correlation between the natural logarithm of BPB in subplots and R_s on 3 November (1 day before trench treatment) when we analyzed separately in plot 1 ($p = 0.327$), plot 2 ($p = 0.365$), and plot 4 ($p = 0.199$), but the relationship was significant in plot 3 (Spearman's rank correlation coefficient = 0.75, $p = 0.038$). However, there was a significant positive correlation ($p = 0.002$–0.003) when data in all subplots were analyzed together (Fig. 6).

Average R_s values in control and pre-trenched plots on 3 November 2020 were 0.58 ± 0.06 and 0.57 ± 0.15 μmol CO_2 m^{-2} s^{-1} in plot 1, 1.69 ± 0.21 and 1.66 ± 0.30 μmol CO_2 m^{-2} s^{-1} in plot 2, 1.04 ± 0.09 and 1.11 ± 0.24 μmol CO_2 m^{-2} s^{-1} in plot 3, and 0.64 ± 0.23 and 0.62 ± 0.16 μmol CO_2 m^{-2} s^{-1} in plot 4, respectively (mean ± SE, n = 4, 5, 3, and 4 for plots 1–4, Fig. 7a). Average soil CO_2 efflux (F_c) values measured in control and trenched plots 15 days after trench treatment on 19 November were 1.23 ± 0.40 and 0.58 ± 0.03 μmol CO_2 m^{-2} s^{-1} in plot 1, 1.69 ± 0.24 and 0.98 ± 0.07 μmol CO_2 m^{-2} s^{-1} in plot 2, 0.90 ± 0.19 and 0.31 ± 0.03 μmol CO_2 m^{-2} s^{-1} in plot 3, and 1.29 ± 0.35 and 0.49 ± 0.13 μmol CO_2 m^{-2} s^{-1} in plot 4, respectively (mean ± SE, n = 4, 5, 3, and 4 for plots 1–4, Fig. 7b). Based on the F_c data collected on 19 November, R_{a_50}/R_s was calculated as 0.53, 0.42, 0.65, and 0.62 in plots 1–4, respectively.

Soil organic carbon and microbial abundance. Total SOC stocks from 0 to 30 cm depth in plots 1–4 were 44.5 ± 1.5, 57.9 ± 3.6, 248.5 ± 30.5, and 328.2 ± 73.2 g C m^{-2} (mean ± SE, $n = 3$), respectively. The ratio of SOC stock in the upper 10 cm against SOC stock to a depth of 30 cm in plots 1 to 4 were 31%, 26%, 48%, and

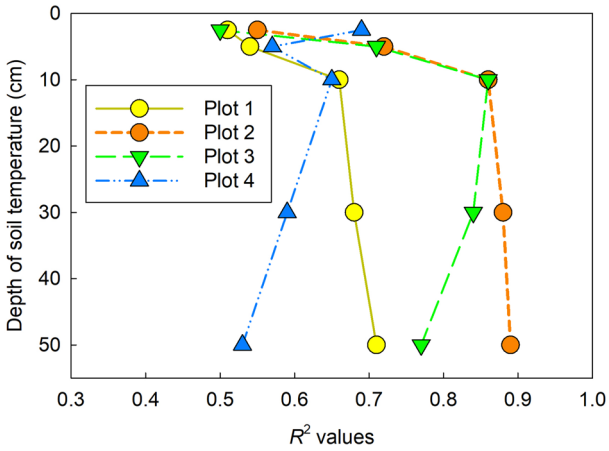

Figure 2. Change of R^2 values based on the relationships between soil temperature at each depth and average R_s in each plot. For this analysis, data for late August were removed to avoid the period of drought stress. Data were measured continuously using an environmental measurement system and standalone soil temperature sensors near each plot at depths of 5, 10, and 30 cm. Soil temperature at the depth of 0–5 cm was measured simultaneously with R_s at each measurement point. Soil temperature at a depth of 50 cm was the reference soil temperature at the center of plot 3. This figure was created using Sigmaplot 14.5 software (Systat Software, San Jose, CA, USA, https://systatsoftware.com/sigmaplot/).

61%, respectively. Total nitrogen stocks at 0 to 30 cm depth in plots 1–4 were 7.8 ± 0.7, 7.1 ± 0.3, 14.3 ± 1.1, and 13.5 ± 1.6 g N m^{-2} (mean ± SE, $n = 3$), respectively.

When averaged across soil depths, plots 3 and 4 had higher bacterial and fungal abundance than the other plots, whereas the bare plot (plot 1) showed the lowest bacterial and fungal abundance (Fig. 8a,b). Soil depth did not have significant effects on either bacterial or fungal abundance, but there were significant interactions between location and soil depth. Deeper soils (20–30 cm) only in plot 4 showed significantly lower microbial abundance when compared to the surface layer. Fungal abundances were from 5 to 125 times lower than bacterial abundances (Fig. 8c). There were significantly positive relationships between SOC stock (g C m^{-2}) and log copies of genes for both bacteria ($R^2 = 0.39$, $p < 0.001$) and fungi ($R^2 = 0.55$, $p < 0.001$).

Discussion

Our study showed that seasonal dynamics of R_s in a coastal dune ecosystem were controlled mainly by soil temperature, except for the dry summer period in August 2020. Generally, the soil temperature is the primary factor controlling R_s in many natural ecosystems[12,22,23]. Gao et al.[15] also reported a strong relationship between soil temperature and R_s in subtropical coastal dunes in China. In most cases, soil temperature at shallower layers (e.g., 5 cm) is the appropriate parameter to explain the dynamics of R_s using exponential regressions[24–26], because the litter layer and shallow layers of soil (e.g., A horizon), which contain more SOC than the deeper layer, contributes a large portion of the total R_s[27–29]. Pavelka et al.[30] showed that R^2 values based on an exponential relationship between soil temperature and R_s decreased significantly at greater soil temperature depths in a Norway spruce forest and a mountain grassland in the Czech Republic. However, in plots 1 and 2 in our study, soil temperature at depths of 30 and 50 cm was a better indicator (the best fit soil temperature-depth) than that at 0–5 and 5 cm for seasonal dynamics of R_s (Fig. 2). Our result implies that the difference in best-fit soil temperature depth reflects the vertical distribution of the source of R_s along across soil depth. At least in plots 1 and 2, both the upper layer (above 30 cm) as well as the deeper layer (below 30 cm) appeared to contribute to R_s because BPB was distributed at depths of 200 cm and more (Fig. 5). In plots 3 and 4, on the other hand, 82–95% of BPB was concentrated within the top 30 cm. In addition, 48–61% of SOC was concentrated in the upper 10 cm in plots 3 and 4. Furthermore, the abundances of bacteria and fungi were both significantly higher in the upper 20 cm than at 30-cm depth in plot 4 (Fig. 8). These findings indicate that the shallower soil layer (above 30-cm depth) made a greater contribution to R_s in plots 3 and 4 as compared to that in the other plots, which may explain why soil temperature in the shallower layers (0–5 and 10 cm) fit the soil temperature response model of R_s well in plots 3 and 4. Most previous studies used surface soil temperature (0–10 cm) to examine the soil temperature response of R_s—even in desert ecosystems where extreme surface soil temperatures of > 50 °C were observed[31]. Therefore, when performing temperature response analysis of R_s, we recommend measuring soil temperature at multiple depths, including those at 30 cm and deeper in places where extreme soil temperature variation is expected, such as coastal dunes and deserts.

Soil moisture also had a strong impact on R_s especially in the drought period in August 2020, when a lack of precipitation contributed to drought stress and decreased soil moisture. Coastal dune ecosystems are easily influenced by drought stress[32,33] because of the low water-holding capacity of sand[34]. Under drought stress, R_s is suppressed because of the limited microbial and plant activity, and R_h is expected to be more sensitive to drought stress than R_a[35]. In our study, R_s markedly decreased in plots 3 and 4 under drought stress. There are few reports regarding the effect of drought stress on R_s in the coastal dune ecosystem, but our result for the soil

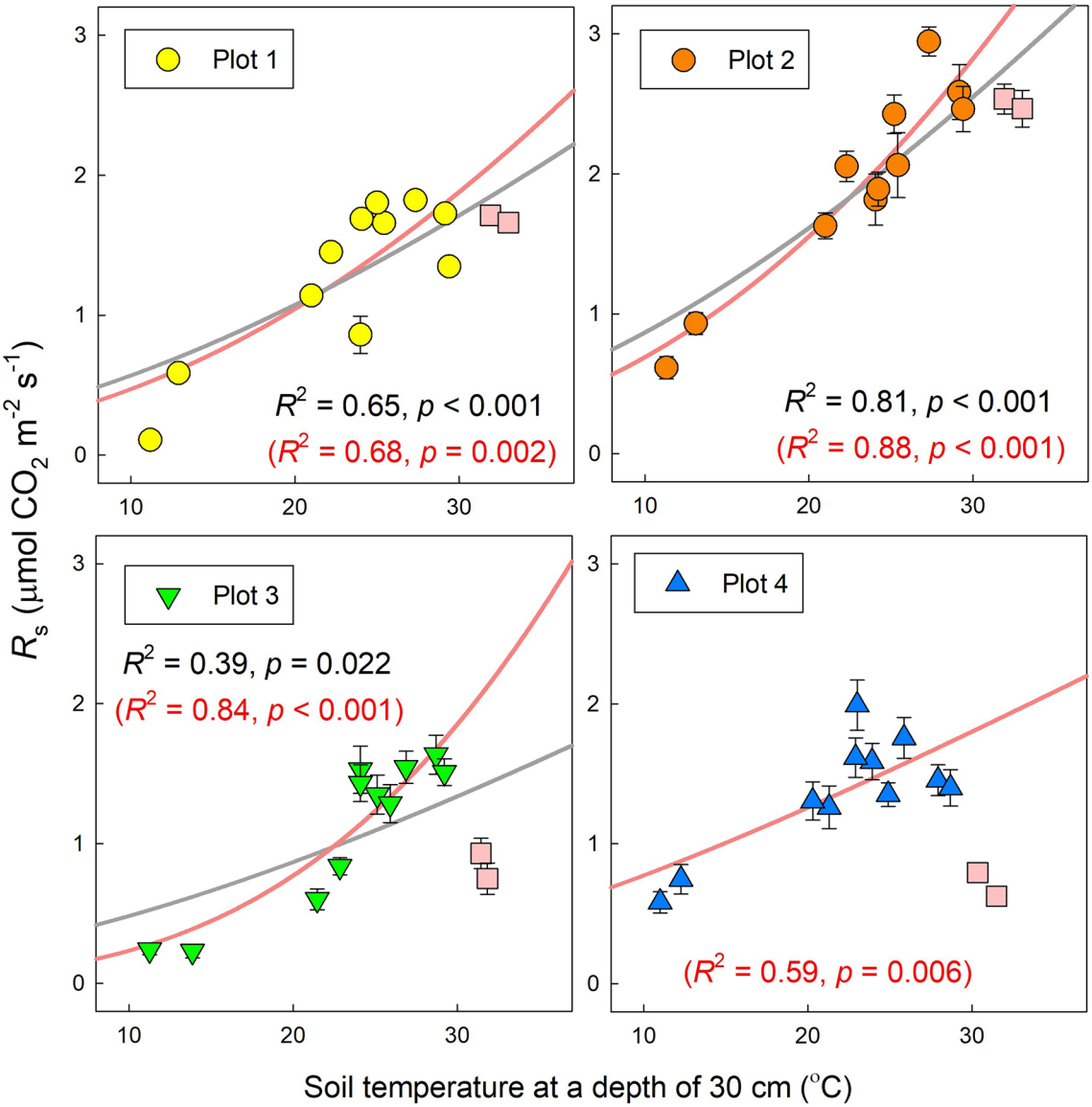

Figure 3. Relationships between soil temperature at 30 cm depth and averaged R_s in each plot. Pink squares represent data in late August 2020. Gray lines with black R^2 and p values, show regression lines obtained by fitting Eq. (3) to all data ($R_s = R_{ref} e^{E_0 \times \left(\frac{1}{T_{ref} - T_0} - \frac{1}{T_s - T_0}\right)}$). Red lines with red R^2 and p values, are those obtained by excluding data from late August during the drought period. Bars show the standard error of the mean ($n = 10$). This figure was created using Sigmaplot 14.5 software (Systat Software, San Jose, CA, USA, https://systatsoftware.com/sigmaplot/).

moisture response of R_s (a mountain-shaped relationship) is consistent with previous studies in several other types of ecosystems[13,28]. Compared with plots 3 and 4, however, R_s was not remarkably decreased in plots 1 and 2 (Fig. 1b). The variety of rooting depths in each plot provides a clue about the difference. BPB in plots 1 (200-cm depth) and plot 2 (> 220 cm) was distributed more deeply than in plots 3 and 4, where more than 90% of BPB was in the upper 50 cm (Fig. 5). Therefore, the deeper rooting depth may have contributed to continued plant activity despite the drought stress at the surface and prevented a decrease of R_a in plots 1 and 2. Our findings indicate that the soil moisture response of R_s differed among vegetation zones of the coastal dune ecosystem, and drought stress markedly decreased R_s in some plots. Data from multiple years will be needed to confirm whether such drought stress occurs frequently in this coastal dune ecosystem because the precipitation in August 2020 was unusually limited compared with that in other years.

The significant positive relationship between the natural logarithm of BPB to 50-cm depth and R_s in November in our study suggests that the distribution of BPB is one factor controlling the spatial dynamics of R_s in the coastal dune ecosystem (Fig. 6). Positive linear relationships between root biomass and R_s have been reported[36–38], whereas our result showed an logarithmic relationship between BPB and R_s. This logarithmic relationship is reasonable when we consider that root respiration exponentially decreases with the increase of root diameter[17,39].

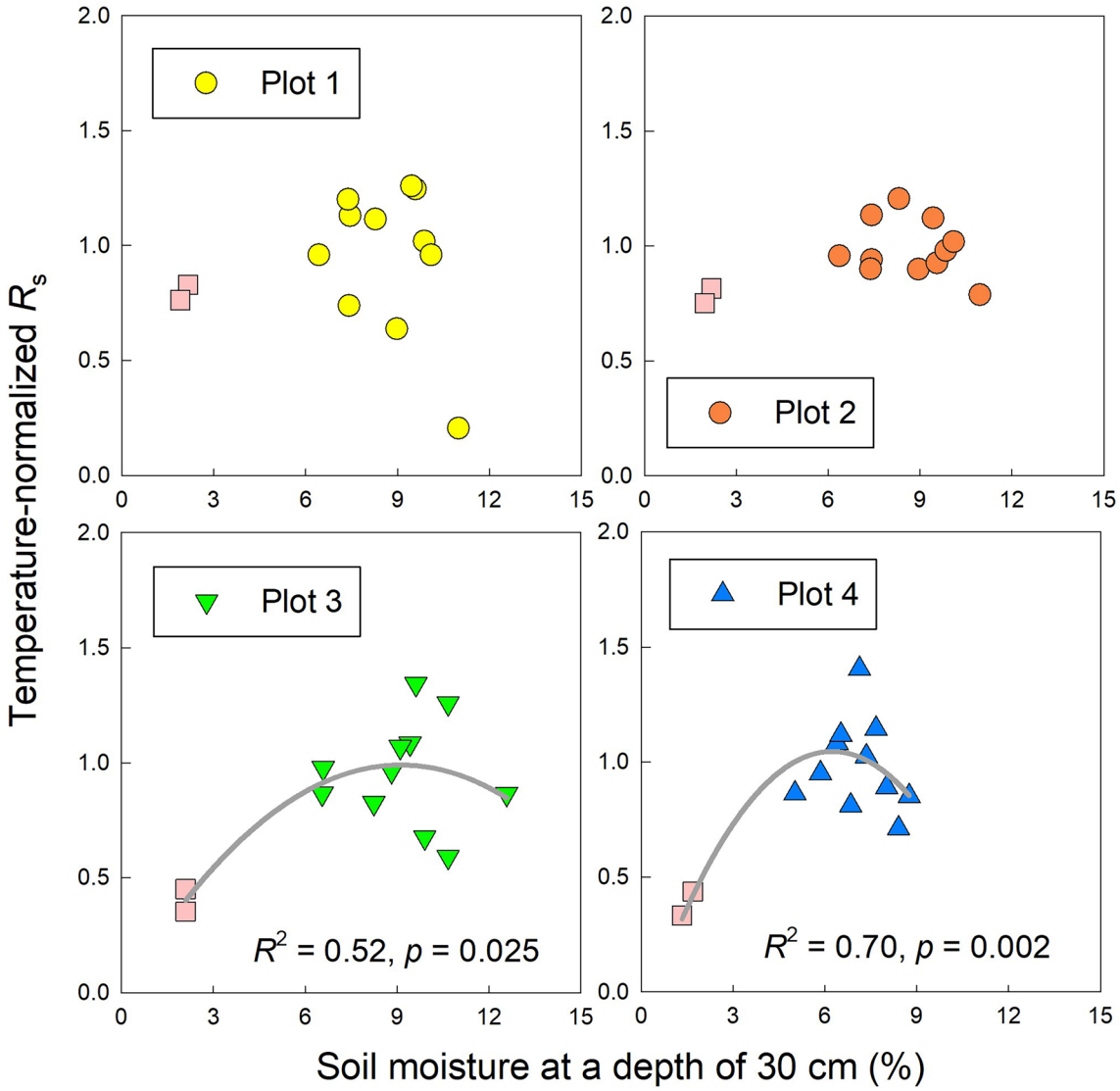

Figure 4. Relationships between soil moisture at a depth of 30 cm and temperature-normalized soil respiration (R_{sN}, observed R_s/modeled R_s) in each measurement plot. Gray lines show significant ($p < 0.05$) relationships between soil moisture and R_{sN} fitted with Eq. (4) ($R_{sN} = c_1\theta^2 + c_2\theta + c_3 (c_1 < 0)$). Pink squares represent R_{sN} during the drought period. This figure was created using Sigmaplot 14.5 software (Systat Software, San Jose, CA, USA, https://systatsoftware.com/sigmaplot/).

Lee[40] reported an logarithmic relationship between root biomass and R_s using field-grown maple seedlings in central Korea. Our findings suggest that such an logarithmic relationship between root biomass and R_s is also applicable to coastal dune ecosystems.

The R_a/R_s to a depth of 50 cm was estimated as 0.42–0.65 in November (Fig. 7). Although information about the R_a/R_s is limited in coastal dune ecosystems, a study by Chapman[17] in nine heathlands, including three dune-heath ecosystems, can serve as a reference. Chapman estimated that root respiration contributed up to 70% of R_s in heathland ecosystems, which is comparable to our result, suggesting that R_a is a large component of R_s in the SOC-limited dune ecosystem. Together, these results suggest that the distribution of BPB and the resulting R_a are major contributors to the spatial dynamics of R_s in coastal dune ecosystems.

In addition to plant roots, the mycorrhizal fungal network also contributes to R_s. For example, Hogberg et al.[41] reported a 50% decrease of R_s as a result of large-scale forest girdling, and they suggested the decrease was due to the inhibition of carbon translocation from host trees to the ectomycorrhizal root tips and mycelia. Ashkannejhad and Horton[42] showed that ectomycorrhizal symbiosis functions as a critical factor for pine establishment in the coastal dune ecosystem in Oregon. In our study, fungal abundance and the fungal/bacterial ratio were highest in the 0–10 cm layer in plot 4 (Fig. 8b,c), near a pine forest. Although it is not possible to separately evaluate the contributions of root respiration and mycorrhizal CO_2 efflux to R_s in our study, this finding implies a possible contribution of ectomycorrhizal root tips and mycelial networks to R_s. The R_a/R_s to a depth of 50 cm was 0.62 in plot 4, and some fraction of the contribution would be caused by ectomycorrhizal CO_2 efflux.

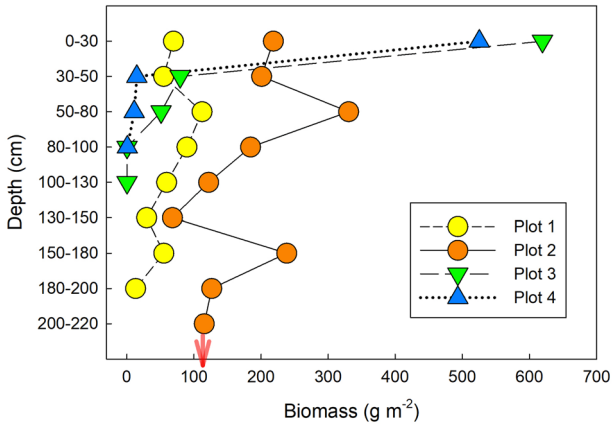

Figure 5. Profile of belowground plant biomass in each measurement plot to depths of 100–220 cm from 18 May to 8 June 2021 ($n = 1$). The red arrow indicates that roots were distributed below 220-cm depth. This figure was created using Sigmaplot 14.5 software (Systat Software, San Jose, CA, USA, https://systatsoftware.com/sigmaplot/).

SOC is the source of R_h and also strongly influences R_s. For example, a study by Li et al.[43] in an alpine meadow ecosystem on the Qinghai-Tibetan Plateau indicated positive relationships between SOC and R_s and their components (R_h and R_a). Morisada et al.[44] estimated the average SOC stock in Japanese forests to a depth of 30 cm as 9.0 kg C m^{-2}. Compared with that amount, the SOC stock at our study site (maximum 0.3 kg C m^{-2} in plot 4) was remarkably limited. Therefore, the relatively small contribution of R_h to R_s is theoretically possible under the SOC-limited condition of our study site. Our microbial analyses revealed a variety of bacterial and fungal abundance in each plot (Fig. 8), suggesting that the contribution of R_h to R_s varies among plots. Our result indicates that the zonal distribution of plant species in a coastal dune ecosystem significantly influenced the abundance of the soil microbiota. In addition, the significantly greater abundance of microbiota and SOC in the shallower layers (0–10 and 10–20 cm) compared with the deeper layer (20–30 cm) in plot 4 suggest that the shallower layer is a larger source of R_h compared with the deeper layer.

There are uncertainties regarding our findings on the influence of BPB on R_s. First, trench treatment in our study was limited to the depth of 50 cm, and we could not exclude the influence of roots in the deeper layer. The influence was likely relatively minor in plots 3 and 4 because more than 90% of BPB was concentrated in the upper 50 cm in those plots (Fig. 5). In plots 1 and 2, however, BPB was distributed at depths greater than 50 cm (Fig. 5), which certainly caused underestimation of the contribution of R_a to R_s in plots 1 and 2. We have limited information regarding the magnitude of the R_a/R_s in deeper layers as compared with that in shallower layers. Pregitzer et al.[45] reported that root respiration in the surface layer (0–10 cm) was up to 40% higher than that at 20- to 30-cm and 40- to 50-cm depth in sugar maple forests in Michigan. According to the report, it is possible that R_a in the deeper layer below 50 cm less contributed to R_s compared with the R_a in the shallower layer (0–50 cm) in our study. Even though, there is no report showing the influence of deeper roots below 50 cm on R_s compared with the roots in the shallower layer. Therefore, the uncertainty of the R_a/R_s in plots 1 and 2 is larger than that in plots 3 and 4.

Second, there is uncertainty about the influence of dead root decomposition and disturbance by trench treatment on R_s in trenched plots, and this may also have caused an underestimation of the R_a/R_s. Carbon input as dead roots to trenched plots is inevitable in the trench treatment[6]. Some studies applied a correction for R_a/R_s by conducting root bag experiments[46,47], whereas others did not[23,48]. In our study, we did not apply any correction for the influence of BPB on R_s because of the short experimental period (we collected root samples to a depth of 50 cm in all subplots within 2 months after trench treatment). Previous studies reported that the influence of disturbance accompanied by trench treatment ceased several months after the treatment[47,49]. For example, Lee et al.[47] reported that F_c of trenched plots was higher compared with that of control plots until 1–2 months after trench treatment, and F_c in trenched plots significantly decreased after that period. In our study, the significant decrease of F_c in trenched plots compared with control plots was confirmed 15 days after trench treatment. It appears that the early occurrence of a F_c decrease after trench treatment was due to the relatively low soil temperature in November (Fig. 1a), such that the influence of dead root decomposition on F_c might be minor.

Third, seasonal dynamics of the R_a/R_s were not considered in this study. Previous studies reported that the R_a/R_s in the growing season was larger than that in the dormant season[50–52]. However, Lee et al.[47] observed an exceptionally large contribution of R_a to R_s in November (71%) in a cool-temperate deciduous forest in central Japan. Our measurement to assess the R_a/R_s was conducted in November, the transitional period from the growing season to the dormant season. Because we did not consider seasonal trends in our estimation of the R_a/R_s in a coastal dune ecosystem, this may have led to under-or overestimation.

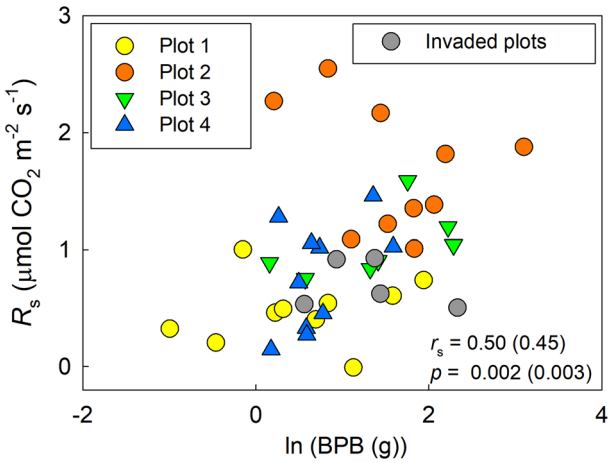

Figure 6. Relationship between the natural logarithm of belowground plant biomass (BPB, g) to a depth of 50 cm in each subplot and R_s on 3 November before trench treatment. Values in the figure are Spearman's rank correlation coefficient (r_s) and p value; values in parentheses are those when we included invaded plots (gray circles) in the analysis. This figure was created using Sigmaplot 14.5 software (Systat Software, San Jose, CA, USA, https://systatsoftware.com/sigmaplot/).

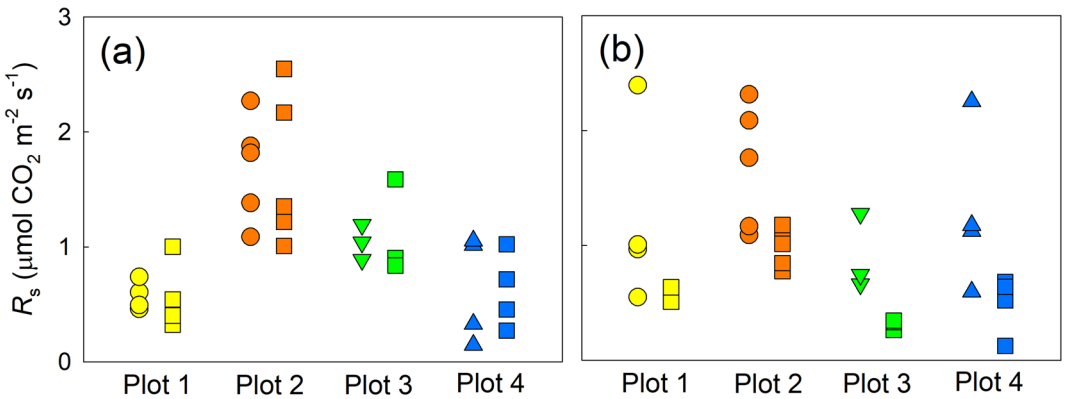

Figure 7. Comparison of R_s values between control and trenched plots (**a**) on 3 November before trench treatment and (**b**) on 19 November, 15 days after trench treatment (n = 4, 5, 3, and 4 for plots 1–4, respectively). R_s data in pre-trenched and trenched plots are shown as squares in all plots. Circles and triangles are R_s data in control plots. This figure was created using Sigmaplot 14.5 software (Systat Software, San Jose, CA, USA, https://systatsoftware.com/sigmaplot/).

Conclusion

The dynamics of R_s were greatly influenced by abiotic and biotic factors in a coastal dune ecosystem. Our findings demonstrated that seasonal dynamics of R_s were controlled by soil temperature, but drought stress also strongly influenced R_s in the dry summer period, and the response of R_s to drought varied among plots dominated by different vegetation species. In addition, R_a made a large contribution to R_s, and the distribution of BPB appeared to be a factor controlling the spatial dynamics of R_s. Furthermore, the microbial analysis suggested that the zonal distribution of vegetation in the dunes also strongly influenced microbial abundance, indicating that the contribution of the microbial community to R_s likely differs among measurement plots. These findings support our hypothesis that relationships between the abiotic and biotic controlling factors and R_s vary among plots dominated by different vegetation species, reflecting the zonal vegetation distribution patterns in a coastal dune ecosystem. Our study provides important data for further examination of coastal dune ecosystems from the viewpoint of carbon cycle analysis.

Materials and methods

Site description. The study site (about 1 ha) is within a coastal dune ecosystem (35° 32′ 26.0″ N, 134° 12′ 27.5″ E) located at the Arid Land Research Center of Tottori University, Tottori, Japan. The mean annual temperature is 15.2 °C, and the mean total precipitation is 1931 mm, based on records collected from 1991 to 2020 at the Tottori observation station of the Japan Meteorological Agency. Dominant plant species around the measure-

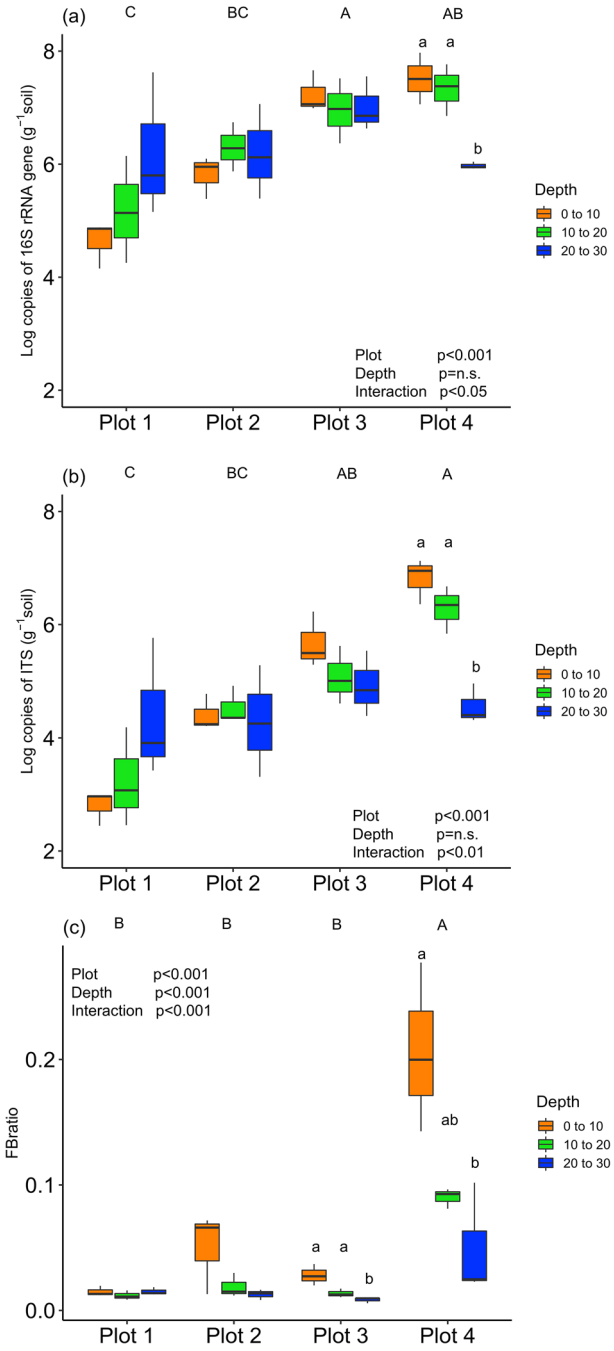

Figure 8. Gene abundances of (**a**) bacteria and archaea, (**b**) fungi, and (**c**) the ratio of fungi and bacteria. The level of significance was determined by two-way ANOVA. Uppercase letters indicate a statistically significant difference between vegetation plots when we averaged the values across soil depth (0–30 cm) and used the Tukey–Kramer test among vegetation plots. Lowercase letters indicate a significant difference between soil depths in each plot.

ment plot were *Vitex rotundifolia* and *Artemisia capillaris*. *Carex kobomugi* and *Ischaemum anthephoroides* were also scattered around the coastal side of the study site, and planted *Pinus thunbergii* trees cover the inland side.

Experimental design. In May 2020, we established four measurement plots at the study site (Fig. 9). Plot 1 was a gap area surrounded by *V. rotundifolia* seedlings. Plot 2 consisted of clusters of *V. rotundifolia* seedlings and was adjacent to plot 1. Within plots 1 and 2, *C. kobomugi* and *I. anthephoroides* were also scattered. Plot 3 was in a mixed area of *V. rotundifolia* and *A. capillaris*; this plot was in the center of the study site. Plot 4 was located in front of *P. thunbergii* trees and was in the most inland area of the study site. On 10 June 2020, we set an environmental measurement system at the center of the study site adjacent to plot 3, and we then obtained continuous data for soil temperature and soil moisture. In each plot (main plot), we set 10 plastic (polypropylene) collars

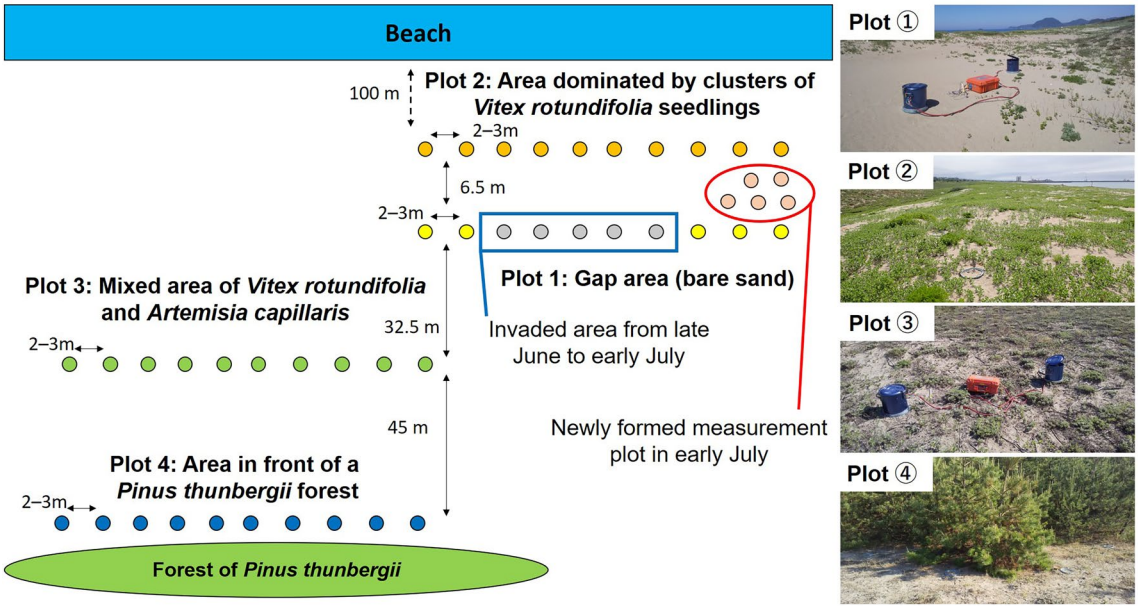

Figure 9. Diagram and photos of measurement plots in the focal coastal dune ecosystem. *Vitex rotundifolia* and *C. kobomugi* invaded a part of plot 1 in late June to early July, after the first R_s measurement on 15 June. Therefore, we set new measurement points for plot 1 in early July.

($n = 10$) before the start of the R_s measurement. We measured R_s every 2 weeks from 15 June to 2 December 2020 in the main plots. *Vitex rotundifolia* and *C. kobomugi* invaded a part of plot 1 in late June and early July, after the first R_s measurement on 15 June. Therefore, we set new measurement points for plot 1 in early July (Fig. 9), and flux calculations for plot 1 were conducted after removing data from the invaded area measured on June 15.

Environmental measurement system. The environmental measurement system was composed of a data logger (CR1000, Campbell Scientific Inc., Logan, UT, USA), battery (SC dry battery, Kind Techno Structure Co. Ltd, Saitama, Japan), solar panel (RNG-50D-SS, RENOGY International Inc., Ontario, CA, USA), charge controller (Solar Amp mini, CSA-MN05-8, DENRYO, Tokyo, Japan), thermocouples (E type), and soil moisture sensors (CS616, Campbell Scientific Inc.). The data logger, battery, and charge controller were kept in a plastic box to avoid exposure to rainfall and sand. Each end of the thermocouple was inserted into a copper tube (4-mm inner diameter, 5-cm length) and affixed with glue. To measure the reference soil temperature at different depths, copper tubes enclosing E-type thermocouples were buried horizontally in the sand at depths of 5, 10, 30, and 50 cm ($n = 1$ for each depth) at the center of plot 3 as reference soil temperature (the data was recorded every 30 min). In addition, we set stand-alone soil temperature sensors (Thermochron SL type, KN Laboratories, Inc. Osaka, Japan) at the center of plots 1 and 4 at depths of 5, 10, and 30 cm ($n = 1$ for each plot, each depth), and they recorded soil temperature data every 30 min. Reference soil temperature at the depth of 5, 10, and 30 cm was used for gap-filling for soil temperature measured by stand-alone sensors at each depth and plot. Soil moisture sensors were buried horizontally in the sand at a depth of 30 cm in the center of plots 1, 3, and 4 ($n = 1$ for each plot) and recorded data every 30 min. Raw values of soil moisture sensors were converted to volumetric soil moisture (%) using a calibration line from 0 to 15% measured in the laboratory using dune sand and three sensors (CS616) referring to the procedure of Bongiovanni et al.[53]. Data for precipitation at the local meteorological observatory in Tottori was downloaded from the home page of the Japan Meteorological Agency (https://www.data.jma.go.jp/gmd/risk/obsdl/index.php).

R_s measurement in the main plots. Polypropylene collars (30-cm inner diameter, 5-cm depth, $n = 10$) were set in each measurement plot in late May 2020. The first R_s measurement was conducted on 15 June 2020. However, *V. rotundifolia* and *C. kobomugi* then invaded about half of the gap area of plot 1, so on 1 July we set 5 new polypropylene collars for plot 1 to replace the 5 invaded measurement points (Fig. 9). The second R_s measurement was conducted on 2 July, and all polypropylene collars then remained in the same position until the end of the measurement period.

R_s was measured using an automated closed dynamic chamber system[54] composed of two cylindrical aluminum chambers (30 cm diameter, 30 cm height) equipped with thermistor temperature sensors (44006, Omega Engineering, Stanford, CA, USA) for measuring air temperature inside the chamber during R_s measurement. Those chambers were connected to a control box equipped with a pump, data logger (CR1000, Campbell Scientific Inc.), CO_2 analyzer (Gascard NG infrared gas sensor, Edinburgh Sensors, Lancashire, UK), and thermometer (MHP, Omega Engineering). The composition of the control box is basically the same as used in previous studies[54,55]. The measurement period for each point was 3 min, and the CO_2 concentration and air temperature inside the chamber were recorded every 5 s. During the measurement, another chamber was set on the next

polypropylene collar with the lid opened, and the next measurement was started at that moment of finishing the previous measurement by automatically closing the chamber lid on the next polypropylene collar in the same plot. Soil temperature at a depth of 0–5 cm was recorded simultaneously by inserting the rod of the thermometer vertically into the soil surface near the polypropylene collar (about 1–2 m from the collar).

R_s was calculated by using the following equation:

$$R_s = \frac{PV}{RS(T_{air} + 273.15)} \frac{\partial C}{\partial t}, \quad (1)$$

where P is the air pressure (Pa), V is the effective chamber volume (m^3), R is the ideal gas constant (8.314 Pa m^3 K^{-1} mol^{-1}), S is the soil surface area (m^2), T_{air} is the air temperature inside the chamber (°C). $\partial C/\partial t$ is the rate of change of the CO_2 mole fraction (μmol mol^{-1} s^{-1}), which was calculated using least-squares regression of the CO_2 changes inside the chamber[12]. For the flux calculation, we removed data for the first 35 s (dead band) of each measurement as an outlier.

Trench treatment and soil CO_2 efflux (F_c) measurement in subplots. In November 2020, we conducted root-cut treatment (trench treatment) in subplots using polyvinyl chloride (PVC) tubes to estimate the contribution of R_a to R_s in the soil layer above 50 cm in each plot (R_{a_50}/R_s). Small PVC collars (10.7 cm inner diameter, 5 cm depth, $n = 10$ for each plot), with the upper ends about 1–2 cm above the soil surface, were set in subplots adjacent to the main plots on 23 October 2020. R_s was measured in subplots using two cylindrical mini PVC chambers (11.8 cm inner diameter at the bottom, 30 cm height, equipped with the same thermistors as cylindrical aluminum chambers for air temperature measurement) connected to the same control box as used for R_s measurement in the main plots. The measurement period was 3 min, and the measurement procedure and the flux calculation were the same as the main plot. R_s was first measured in subplots on 3 November to examine the spatial variation of R_s before trench treatment. Using the data, we selected subplots to conduct trench treatment and control plots for comparison, while aiming to achieve a minimal difference in the average R_s between control and pre-trenched plots. On 4 November, we inserted PVC tubes (10.7 cm inner diameter, 50 cm length) into about half ($n = 3$–5) of the subplots (the same position as PVC collars were set on 23 October) by using a hammer and aluminum lid until the upper end of each PVC tube was 1–2 cm above the soil surface to exclude roots to a depth of about 50 cm. On 19 November, after 15 days of trench treatment, respiration was measured in the same subplots.

The R_{a_50}/R_s was calculated as follows:

$$R_{a\_50}/R_s = (F_{c\_control} - F_{c\_trenched})/F_{c\_control}, \quad (2)$$

where $F_{c\_trenched}$ and $F_{c\_control}$ ($= R_s$) are the F_c values in trenched and control plots on 19 November, respectively.

In late December 2020, all the belowground plant biomass (BPB) in subplots (control and trenched plots) to a depth of 50 cm was collected for biomass analysis, about 2 months after trench treatment. In the laboratory, all the collected plant materials were washed and oven-dried for 72 h at 70 °C, and then the dry weight of the BPB samples was measured.

Biomass measurement. We conducted BPB analysis from 18 May to 8 June 2021 in each plot ($n = 1$). At that time, 100 cm × 100 cm sampling plots near the CO_2 measurement plots (100 cm × 100 cm for plots 2–4 and 50 cm × 50 cm in plot 1 because of the narrow gap area) were dug to a depth of 100–220 cm, according to the root distribution in each plot, and all plant materials were collected by passing the soil through 5- to 7-mm sieves. Once we reached a depth where no roots were visible, no more digging was conducted. In plots 2 and 3, stolons of *V. rotundifolia* were difficult to distinguish from roots if underground. Therefore, we defined plant material as BPB if it was underground. In the laboratory, all of the collected plant materials were washed and air-dried at room temperature for 0–6 days depending on the biomass. After that, samples were oven-dried for 15–25 h at 70–80 °C, and the dry weight of those samples was then measured.

Soil organic carbon and nitrogen. On 21 October 2020, soil pits were dug to a depth of 50 cm near each plot ($n = 3$), and soil core samples were collected. Cylindrical stainless core samplers (5 cm diameter, 5 cm height, 100 cc) were horizontally inserted into the soil pit at depths of 0–5, 5–10, 10–20, and 20–30 cm. In the laboratory, soil core samples were weighed and oven-dried at 105 °C for 48 h, and the dry weight was measured. Oven-dried soil samples were sieved with a 2-mm-pore stainless wire mesh screen, and visible fungal mycelia in soil samples from plot 4 were removed as well as possible. Sieved samples were ground with an agate mortar. Samples (fine powder) were oven-dried for 24 h at 105 °C and weighed before SOC and nitrogen analysis. About 1.5 g of powdered samples were used for the analysis. Organic carbon content (combustion at 400 °C) and total nitrogen in samples were analyzed using a Soli TOC cube (Elementar Analysensysteme GmbH, Langenselbold, Germany) by the combustion method.

Microbial abundance. On 21 October 2020, soil samples for microbial analysis were collected at the same time as soil core sampling for SOC and nitrogen analysis. Soil samples were collected at depths of 0–10, 10–20, and 20–30 cm using a stainless spatula and placed individually in a polyethylene bag. The bags were kept in a cooler box with ice in the field and then placed in a freezer (– 30 °C) in the laboratory soon after sampling.

DNA was extracted from 0.5 g of the fresh soils using NucleoSpin Soil (Takara Bio, Inc., Shiga, Japan) according to the manufacturer's instructions (SL1 buffer), and the extracts were stored at – 20 °C until further analysis. Bacterial and archaeal 16S rRNA and fungal internal transcribed spacer (ITS) gene were targeted to investigate

the microbial abundance. Bacterial and archaeal 16S rRNA (V4 region) and fungal ITS were determined using the universal primer sets 515F/806R and ITS1F_KYO2/ITS2_KYO2, respectively[56,57].

For qPCR, samples were prepared with 10 µL of the KAPA SYBR Fast qPCR kit (Kapa Biosystems, Wilmington, MA, USA), 0.8 µL of forward primer, 0.8 µL of reverse primer, and 3 µL of 1–50 × diluted soil DNA. Nuclease-free water was added to make up to a final volume of 20 µL. Cycling conditions of 16S rRNA were 95 °C for 30 s, followed by 40 cycles at 95 °C for 30 s, 58 °C for 30 s, and 72 °C for 1 min. Cycling conditions of ITS were 95 °C for 30 s, followed by 40 cycles at 95 °C for 30 s, 55 °C for 1 min, and 72 °C for 1 min. A melting curve analysis was performed in a final cycle of 95 °C for 15 s, 60 °C for 1 min, and 95 °C for 15 s. High amplification efficiencies of 99% for bacterial and archaeal 16S rRNA genes and 101% for the fungal ITS were obtained based on the standard curves.

Data analysis. To examine the environmental response (soil temperature and soil moisture) of R_s, nonlinear and quadratic regression models were applied. We conducted *F*-tests by comparing the regression model to a constant model whose value is the mean of the observations (significance set at $p < 0.05$). For the temperature response analysis of R_s, we used the following equation[58]:

$$R_s = R_{ref} e^{E_0 \times \left(\frac{1}{T_{ref} - T_0} - \frac{1}{T_s - T_0}\right)}, \quad (3)$$

where R_{ref} (µmol CO_2 m^{-2} s^{-1}) is the CO_2 efflux at a specified reference soil temperature (T_{ref}: 283.15 K), E_0 is a fitting parameter, T_0 is the soil temperature when R_s is zero (227.13 K), and T_s is the observed soil temperature (K) at different depths (0–5, 5, 10, 30, 50 cm). Based on the 1-year soil moisture data between 11 June 2020 and 10 June 2021, we defined the period when soil moisture was below the annual average − 2SD (= 3.9%) as a drought period (10 August to 4 September), and we conducted nonlinear regression for the temperature response of R_s with and without R_s data during the drought period. To avoid the confounding effects of soil temperature and soil moisture, we first divided the observed value by the simulated value of R_s based on the temperature response curve (the curve was calculated without data collected in late August 2020, during a drought period). The temperature-normalized R_s, R_{sN}, was used to analyze the relationship between soil moisture and R_s[59]. The relationship was fitted with the following quadratic regression:

$$R_{sN} = c_1\theta^2 + c_2\theta + c_3 (c_1 < 0), \quad (4)$$

where θ is the volumetric soil moisture (%) and c_1, c_2, and c_3 are fitting parameters.

To examine the relationship between BPB and R_s, we referred to the logarithmic relationship between root biomass and R_s in a previous study in a forest ecosystem[40], and we calculated the natural logarithm of BPB to a depth of 50 cm (ln BPB (g)). Correlation analysis (Spearman's rank correlation, significance set at $p < 0.05$) between the ln BPB in each subplot and R_s was conducted.

To examine the relationship between SOC stock (g C m^{-2}) and microbial abundance (log copies of genes g^{-1} soil), linear regression analysis and *F*-tests were performed (significance set at $p < 0.05$).

We performed all the above-mentioned statistical analyses using Sigmaplot 14.5 software (Systat Software, San Jose, CA, USA, https://systatsoftware.com/sigmaplot/).

The soil microbial abundance was assessed by using two-way analysis of variance (ANOVA) in R 4.0.3., and then Tukey's test was performed to analyze significant differences between each treatment. Differences were considered statistically significant at $p < 0.05$ (two-sided test).

Ethics statement. The collection of plant materials in this study complied with relevant institutional, national, and international guidelines and legislation.

Data availability

The datasets generated in this study are available from the corresponding author according to reasonable requests from readers.

Received: 19 December 2021; Accepted: 31 July 2022
Published online: 22 August 2022

References

1. Brown, A. C. & McLachlan, A. Sandy shore ecosystems and the threats facing them: Some predictions for the year 2025. *Environ. Conserv.* **29**, 62–77. https://doi.org/10.1017/S037689290200005X (2002).
2. Barbier, E. B. *et al.* The value of estuarine and coastal ecosystem services. *Ecol. Monogr.* **81**, 169–193. https://doi.org/10.1890/10-1510.1 (2011).
3. Directorate-General for Environment (European Commission). *Building a green infrastructure for Europe*. Publications Office of the European Union. https://doi.org/10.2779/54125 (2014).
4. Drius, M., Carranza, M. L., Stanisci, A. & Jones, L. The role of Italian coastal dunes as carbon sinks and diversity sources. A multi-service perspective. *Appl. Geogr.* **75**, 127–136. https://doi.org/10.1016/j.apgeog.2016.08.007 (2016).
5. Raich, J. W. & Schlesinger, W. H. The global carbon-dioxide flux in soil respiration and its relationship to vegetation and climate. *Tellus B* **44**, 81–99. https://doi.org/10.1034/j.1600-0889.1992.t01-1-00001.x (1992).
6. Epron, D. In *Soil Carbon Dynamics: An Integrated Methodology* (eds. Heinemeyer, A., Bahn, M., & Kutsch, W. L.) 157–168 (Cambridge University Press, 2010).
7. Bond-Lamberty, B. & Thomson, A. Temperature-associated increases in the global soil respiration record. *Nature* **464**, 579–582. https://doi.org/10.1038/nature08930 (2010).
8. Bond-Lamberty, B. New techniques and data for understanding the global soil respiration flux. *Earth's Future* **6**, 1176–1180. https://doi.org/10.1029/2018ef000866 (2018).

9. Stell, E., Warner, D., Jian, J., Bond-Lamberty, B. & Vargas, R. Spatial biases of information influence global estimates of soil respiration: How can we improve global predictions?. *Glob. Change Biol.* **27**, 3923–3938. https://doi.org/10.1111/gcb.15666 (2021).
10. Jian, J. *et al.* A global database of soil respiration data, version 5.0. ORNL DAAC, Oak Ridge, Tennessee, USA. https://doi.org/10.3334/ORNLDAAC/1827.
11. Luo, Y. Q., Wan, S. Q., Hui, D. F. & Wallace, L. L. Acclimatization of soil respiration to warming in a tall grass prairie. *Nature* **413**, 622–625. https://doi.org/10.1038/35098065 (2001).
12. Teramoto, M. *et al.* Enhanced understory carbon flux components and robustness of net CO_2 exchange after thinning in a larch forest in central Japan. *Agric. For. Meteorol.* **74**, 106–117. https://doi.org/10.1016/j.agrformet.2019.04.008 (2019).
13. Zhang, X. *et al.* Effects of continuous drought stress on soil respiration in a tropical rainforest in southwest China. *Plant Soil* **394**, 343–353. https://doi.org/10.1007/s11104-015-2523-4 (2015).
14. Harper, C. W., Blair, J. M., Fay, P. A., Knapp, A. K. & Carlisle, J. D. Increased rainfall variability and reduced rainfall amount decreases soil CO_2 flux in a grassland ecosystem. *Glob. Change Biol.* **11**, 322–334. https://doi.org/10.1111/j.1365-2486.2005.00899.x (2005).
15. Gao, W., Huang, Z., Ye, G., Yue, X. & Chen, Z. Effects of forest cover types and environmental factors on soil respiration dynamics in a coastal sand dune of subtropical China. *J. For. Res.* **29**, 1645–1655. https://doi.org/10.1007/s11676-017-0565-6 (2018).
16. Panda, T. Significance of soil properties and microbial activity on soil CO_2 emission in coastal sand dunes of Odisha, India. *J. Indian Bot. Soc.* **100**, 148–159. https://doi.org/10.5958/2455-7218.2020.00036.4 (2020).
17. Chapman, S. B. Some interrelationships between soil and root respiration in lowland calluna heathland in southern England. *J. Ecol.* **67**, 1–20. https://doi.org/10.2307/2259333 (1979).
18. Ishikawa, S.-I., Furukawa, A. & Oikawa, T. Zonal plant distribution and edaphic and micrometeorological conditions on a coastal sand dune. *Ecol. Res.* **10**, 259–266. https://doi.org/10.1007/BF02347851 (1995).
19. Šilc, U. *et al.* Sand dune vegetation along the eastern Adriatic coast. *Phytocoenologia* **46**, 339–355. https://doi.org/10.1127/phyto/2016/0079 (2016).
20. Hwang, J.-S. *et al.* Relationship between the spatial distribution of coastal sand dune plants and edaphic factors in a coastal sand dune system in Korea. *J. Ecol. Environ.* **39**, 17–29. https://doi.org/10.5141/ecoenv.2016.003 (2016).
21. Metcalfe, D. B., Fisher, R. A. & Wardle, D. A. Plant communities as drivers of soil respiration: Pathways, mechanisms, and significance for global change. *Biogeosciences* **8**, 2047–2061. https://doi.org/10.5194/bg-8-2047-2011 (2011).
22. Tan, Z.-H. *et al.* Soil respiration in an old-growth subtropical forest: Patterns, components and controls. *J. Geophys. Res.-Atmos.* **118**, 2981–2990. https://doi.org/10.1002/jgrd.50300 (2013).
23. Teramoto, M., Liang, N., Ishida, S. & Zeng, J. Long-term stimulatory warming effect on soil heterotrophic respiration in a cool-temperate broad-leaved deciduous forest in northern Japan. *J. Geophys. Res-Biogeochem.* **123**, 1161–1177. https://doi.org/10.1002/2018jg004432 (2018).
24. Ruehr, N. K. & Buchmann, N. Soil respiration fluxes in a temperate mixed forest: Seasonality and temperature sensitivities differ among microbial and root-rhizosphere respiration. *Tree Physiol.* **30**, 165–176. https://doi.org/10.1093/treephys/tpp106 (2010).
25. Yan, T. *et al.* Temperature sensitivity of soil respiration across multiple time scales in a temperate plantation forest. *Sci. Total Environ.* **688**, 479–485. https://doi.org/10.1016/j.scitotenv.2019.06.318 (2019).
26. Noh, N. J., Kuribayashi, M., Saitoh, T. M. & Muraoka, H. Different responses of soil, heterotrophic and autotrophic respirations to a 4-year soil warming experiment in a cool-temperate deciduous broadleaved forest in central Japan. *Agric. For. Meteorol.* **247**, 560–570. https://doi.org/10.1016/j.agrformet.2017.09.002 (2017).
27. Fang, C. & Moncrieff, J. B. The variation of soil microbial respiration with depth in relation to soil carbon composition. *Plant Soil* **268**, 243–253. https://doi.org/10.1007/s11104-004-0278-4 (2005).
28. Wang, D., Yu, X., Jia, G., Qin, W. & Shan, Z. Variations in soil respiration at different soil depths and its influencing factors in forest ecosystems in the mountainous area of north China. *Forests* **10**, 1081. https://doi.org/10.3390/f10121081 (2019).
29. Hirano, T., Kim, H. & Tanaka, Y. Long-term half-hourly measurement of soil CO_2 concentration and soil respiration in a temperate deciduous forest. *J. Geophys. Res-Atmos.* **108**, 4631. https://doi.org/10.1029/2003JD003766 (2003).
30. Pavelka, M., Acosta, M., Marek, M. V., Kutsch, W. & Janous, D. Dependence of the Q_{10} values on the depth of the soil temperature measuring point. *Plant Soil* **292**, 171–179. https://doi.org/10.1007/s11104-007-9213-9 (2007).
31. Cable, J. M. *et al.* The temperature responses of soil respiration in deserts: A seven desert synthesis. *Biogeochemistry* **103**, 71–90. https://doi.org/10.1007/s10533-010-9448-z (2011).
32. Novo, F. G., Barradas, M. C. D., Zunzunegui, M., Mora, R. G. & Fernández, J. B. G. In *Coastal Dunes: Ecology and Conservation* (eds Martínez, M. L. & Psuty, N. P.) 155–169 (Springer, 2004).
33. Hesp, P. A. Ecological processes and plant adaptations on coastal dunes. *J. Arid Environ.* **21**, 165–191. https://doi.org/10.1016/S0140-1963(18)30681-5 (1991).
34. Salisbury, E. J. *Downs & Dunes; Their Plant Life and Its Environment* (Bell, 1952).
35. Wang, Y. F. *et al.* Responses of soil respiration and its components to drought stress. *J. Soil. Sediment.* **14**, 99–109. https://doi.org/10.1007/s11368-013-0799-7 (2014).
36. Kucera, C. L. & Kirkham, D. R. Soil respiration studies in tallgrass prairie in Missouri. *Ecology* **52**, 912–915. https://doi.org/10.2307/1936043 (1971).
37. Behera, N., Joshi, S. K. & Pati, D. P. Root contribution to total soil metabolism in a tropical forest soil from Orissa, India. *For. Ecol. Manag.* **36**, 125–134. https://doi.org/10.1016/0378-1127(90)90020-c (1990).
38. Tomotsune, M., Yoshitake, S., Watanabe, S. & Koizumi, H. Separation of root and heterotrophic respiration within soil respiration by trenching, root biomass regression, and root excising methods in a cool-temperate deciduous forest in Japan. *Ecol. Res.* **28**, 259–269. https://doi.org/10.1007/s11284-012-1013-x (2013).
39. Jia, S. X., McLaughlin, N. B., Gu, J. C., Li, X. P. & Wang, Z. Q. Relationships between root respiration rate and root morphology, chemistry and anatomy in *Larix gmelinii* and *Fraxinus mandshurica*. *Tree Physiol.* **33**, 579–589. https://doi.org/10.1093/treephys/tpt040 (2013).
40. Lee, J.-S. Relationship of root microbial biomass and soil respiration in a stand of deciduous broadleaved trees—A case study in a maple tree. *J. Ecol. Environ.* **42**, 19. https://doi.org/10.1186/s41610-018-0078-z (2018).
41. Hogberg, P. *et al.* Large-scale forest girdling shows that current photosynthesis drives soil respiration. *Nature* **411**, 789–792. https://doi.org/10.1038/35081058 (2001).
42. Ashkannejhad, S. & Horton, T. R. Ectomycorrhizal ecology under primary succession on coastal sand dunes: Interactions involving *Pinus contorta*, suilloid fungi and deer. *New Phytol.* **169**, 345–354. https://doi.org/10.1111/j.1469-8137.2005.01593.x (2006).
43. Li, W. *et al.* Nitrogen fertilizer regulates soil respiration by altering the organic carbon storage in root and topsoil in alpine meadow of the north-eastern Qinghai-Tibet Plateau. *Sci. Rep.* **9**, 13735. https://doi.org/10.1038/s41598-019-50142-y (2019).
44. Morisada, K., Ono, K. & Kanomata, H. Organic carbon stock in forest soils in Japan. *Geoderma* **119**, 21–32. https://doi.org/10.1016/S0016-7061(03)00220-9 (2004).
45. Pregitzer, K. S., Laskowski, M. J., Burton, A. J., Lessard, V. C. & Zak, D. R. Variation in sugar maple root respiration with root diameter and soil depth. *Tree Physiol.* **18**, 665–670. https://doi.org/10.1093/treephys/18.10.665 (1998).
46. Diaz-Pines, E. *et al.* Root trenching: A useful tool to estimate autotrophic soil respiration? A case study in an Austrian mountain forest. *Eur. J. For. Res.* **129**, 101–109. https://doi.org/10.1007/s10342-008-0250-6 (2010).

47. Lee, M. S., Nakane, K., Nakatsubo, T. & Koizumi, H. Seasonal changes in the contribution of root respiration to total soil respiration in a cool-temperate deciduous forest. *Plant Soil* **255**, 311–318. https://doi.org/10.1023/A:1026192607512 (2003).
48. Noh, N.-J. *et al.* Responses of soil, heterotrophic, and autotrophic respiration to experimental open-field soil warming in a cool-temperate deciduous forest. *Ecosystems* **19**, 504–520. https://doi.org/10.1007/s10021-015-9948-8 (2016).
49. Bond-Lamberty, B., Bronson, D., Bladyka, E. & Gower, S. T. A comparison of trenched plot techniques for partitioning soil respiration. *Soil Biol. Biochem.* **43**, 2108–2114. https://doi.org/10.1016/j.soilbio.2011.06.011 (2011).
50. Li, X. *et al.* Contribution of root respiration to total soil respiration in a semi-arid grassland on the Loess Plateau, China. *Sci. Total Environ.* **627**, 1209–1217. https://doi.org/10.1016/j.scitotenv.2018.01.313 (2018).
51. Hanson, P. J., Edwards, N. T., Garten, C. T. & Andrews, J. A. Separating root and soil microbial contributions to soil respiration: A review of methods and observations. *Biogeochemistry* **48**, 115–146. https://doi.org/10.1023/A:1006244819642 (2000).
52. Bond-Lamberty, B., Wang, C. K. & Gower, S. T. Contribution of root respiration to soil surface CO_2 flux in a boreal black spruce chronosequence. *Tree Physiol.* **24**, 1387–1395. https://doi.org/10.1093/treephys/24.12.1387 (2004).
53. Bongiovanni, T., Liu, P.-W., Preston, D., Feagle, S. & Judge, J. Calibrating time domain reflectometers for soil moisture measurements in sandy soils: AE519, 2/2017. *EDIS* **2017**, https://doi.org/10.32473/edis-ae519-2017 (2017).
54. Abe, Y. *et al.* Spatial variation in soil respiration rate is controlled by the content of particulate organic materials in the volcanic ash soil under a *Cryptomeria japonica* plantation. *Geoderma Reg.* **29**, e00529. https://doi.org/10.1016/j.geodrs.2022.e00529 (2022).
55. Sun, L., Hirano, T., Yazaki, T., Teramoto, M. & Liang, N. Fine root dynamics and partitioning of root respiration into growth and maintenance components in cool temperate deciduous and evergreen forests. *Plant Soil* **446**, 471–486. https://doi.org/10.1007/s11104-019-04343-z (2020).
56. Caporaso, J. G. *et al.* Global patterns of 16S rRNA diversity at a depth of millions of sequences per sample. *Proc. Natl. Acad. Sci. USA* **108**, 4516–4522. https://doi.org/10.1073/pnas.1000080107 (2011).
57. Toju, H., Tanabe, A. S., Yamamoto, S. & Sato, H. High-coverage ITS primers for the DNA-based identification of *Ascomycetes* and *Basidiomycetes* in environmental samples. *PLoS One* **7**, e40863. https://doi.org/10.1371/journal.pone.0040863 (2012).
58. Lloyd, J. & Taylor, J. A. On the temperature-dependence of soil respiration. *Funct. Ecol.* **8**, 315–323. https://doi.org/10.2307/2389824 (1994).
59. Wang, B. *et al.* Soil moisture modifies the response of soil respiration to temperature in a desert shrub ecosystem. *Biogeosciences* **11**, 259–268. https://doi.org/10.5194/bg-11-259-2014 (2014).

Acknowledgements

We appreciate technical support for the SOC and nitrogen analysis from the Engineering Department of the Arid Land Research Center of Tottori University and advice on the statistical analysis provided by Mr. Ryuji Fukushima (ESUMI Co., Ltd.) and Dr. Shigeaki Ohtsuki (Japan Institute of Statistical Technology). We also express our gratitude to the handling editor and two anonymous reviewers for the detailed insight into our study and constructive comments. This study was funded by a grant from the Tenure-Track Program of Tottori University. This work was also partially funded by the Joint Research Program of Arid Land Research Center, Tottori University (03A2001), by the Environment Research and Technology Development Fund (JPMEERF20202006) of the Environmental Restoration and Conservation Agency of Japan, and by the Nippon Life Insurance Foundation.

Author contributions

M.T. designed the experiment. M.T. and R.H. collected environmental data, biomass data, and soil CO_2 efflux data. T.H. conducted microbial analysis, and T.T. supported the microbial analysis. N.L. developed a soil CO_2 efflux measurement system and supported data collection. N.Y. introduced the study site to M.T. and discussed the experimental design with M.T. M.T. wrote the first draft of the manuscript and T.H., N.L., T.T., T.Y.I., R.H., and N.Y. provided information and feedbacks for revising the manuscript at all stages.

Competing interests

The authors declare no competing interests.

Additional information

Correspondence and requests for materials should be addressed to M.T.

Reprints and permissions information is available at www.nature.com/reprints.

Publisher's note Springer Nature remains neutral with regard to jurisdictional claims in published maps and institutional affiliations.